

Liquid Hopfield model: retrieval and localization in heterogeneous liquid mixtures

Rodrigo Braz Teixeira

*Department of Physics, Faculty of Sciences, University of Lisbon, Lisbon, Portugal and
Institute Gulbenkian of Science, Oeiras, Portugal, [equal contribution]*

Giorgio Carugno

*Department of Mathematics, King's College London, Strand,
London, WC2R 2LS, United Kingdom, [equal contribution]*

Izaak Neri

Department of Mathematics, King's College London, Strand, London, WC2R 2LS, United Kingdom

Pablo Sartori

Institute Gulbenkian of Science, Oeiras, Portugal.

(Dated: November 17, 2023)

Biological mixtures, such as the cellular cytoplasm, are composed of a large number of different components. From this heterogeneity, ordered mesoscopic structures emerge, such as liquid phases with controlled composition. These structures compete with each other for the same components. This raises several questions, such as what types of interactions allow the *retrieval* of multiple ordered mesoscopic structures, and what are the physical limitations for the retrieval of said structures. In this work, we develop an analytically tractable model for liquids capable of retrieving states with target compositions. We name this model the *liquid Hopfield model* in reference to corresponding work in the theory of associative neural networks. By solving this model, we show that non-linear repulsive interactions are necessary for retrieval of target structures. We demonstrate that this is because liquid mixtures at low temperatures tend to transition to phases with few components, a phenomenon that we term *localization*. Taken together, our results demonstrate a trade-off between retrieval and localization phenomena in liquid mixtures.

INTRODUCTION

Within cells, thousands of different components, including proteins, nucleic acids and small peptides, interact with each other [1, 2]. From this heterogeneous mixture, mesoscopic scale ordered structures are *retrieved* to perform specific biological functions. Examples of such retrieval are the assembly of solid-like multi-protein complexes [3], demixing of liquid droplets in the cytoplasm [4–7], or formation of lipid rafts on the membrane [8, 9]. Therefore, the parsimonious coexistence of heterogeneity and order is an essential characteristic of cellular mixtures.

Conventional statistical mechanics and soft matter physics, focuses on systems in which the number of component species, N , is much smaller than the total number of components per species, M . The standard thermodynamic limit is thus $N \ll M$ and $M \rightarrow \infty$. In contrast, biological mixtures often take place in the regime $N, M \rightarrow \infty$, and exhibit ordered phases in which the number of components enriched is also large, $Q \lesssim N$. This alternative thermodynamic limit, elsewhere referred to as multifarious [3, 10], is key for the concurrence of heterogeneity and order in biological matter.

Previous studies of liquid mixtures with many components can be roughly grouped in two categories. The first, pioneered by Sear and Cuesta [1], uses analytical tools to study stability of the homogeneous state of a mixture with random interactions [1, 11–15]. The second, uses numerical inverse optimization on the interactions so to

enforce stability of multiple target phases [16, 17]. However, both approaches have important caveats: the stability properties of the homogeneous phase cannot be used to predict the properties of ordered phases, which are in any case unlikely for random interactions; and while inverse optimization guarantees by construction stability of target phases, it sheds no light into the nature of the interactions that guarantee such stability. Due to these limitations, two central questions remain unanswered: what types of interactions ensure retrieval of target ordered structures, and what are the physical trade-offs of target retrieval in heterogeneous mixtures?

To answer these questions, we follow an alternative approach: we prescribe a set of interactions and analytically derive the conditions under which these guarantee stability of target phases. Our choice of interactions is based on an analogy between the nucleation of target liquid phases and the retrieval of patterns in Hopfield neural networks [18], see also [3, 10]. We thus refer to this model as the *liquid Hopfield model*. For this model, we find conditions to ensure stability of up to $p = N - 1$ target phases, for arbitrary values of N and Q . One key condition is the presence of non-linear repulsive interactions, which stabilize retrieval. We further show that when such non-linearities are weak the mixture tends towards localized phases, in line with prior numerical evidence [11, 12], and show that perfect localization occurs at zero temperature. Overall, this work establishes that multi-component mixtures exhibit a trade-off between lo-

calization and retrieval, with non-linearities playing a key role in leveraging this trade-off.

This paper is organized as follows. In Section I, we summarize the thermodynamics of multi-component liquid mixtures in the grand-canonical ensemble. Section II frames the problem of retrieval in liquid mixtures and defines the interaction matrix which completes the *liquid Hopfield model*. In Sections III-VI we study homogeneous, retrieval and localized states for a particular choice of targets, which we later show to be the worst-case scenario of the *liquid Hopfield model*. Section VII extends our results to arbitrary targets and Section VIII studies the effect of sparsity. Lastly, in Section IX we summarise the results of this paper and put them in the context of current advances in multi-component mixtures.

RESULTS

I. THERMODYNAMICS OF HETEROGENEOUS FLUID MIXTURES

We consider a multi-component fluid mixture of N molecular species with densities ρ_i , where $i = 1, 2, \dots, N$. The thermodynamic behavior of this fluid is dictated by the free energy density

$$f(\vec{\rho}, T) = u(\vec{\rho}) - T s(\vec{\rho}), \quad (1)$$

where u is the energy density, s is the entropy density [19], and T is the temperature; curly brackets denote the vector of all densities.

A generic form for the entropy density can be obtained by adding the entropy of each of the components to that of the solvent, see e.g. Refs. [11, 20–22]. The resulting expression is

$$s(\vec{\rho}) = -k_B \sum_{i=1}^N \rho_i \log(\rho_i) - k_B(1 - \rho) \log(1 - \rho), \quad (2)$$

where k_B is Boltzmann's constant (in what follows we set $k_B T = 1$) and $\rho = \sum_{i=1}^N \rho_i$ the total density. Nota bene, the entropy diverges for $\rho_i = 0$ or $\rho = 1$, which constrains the densities to the interior of the $N - 1$ dimensional standard simplex.

We characterize the internal energy via a low-density expansion and truncate to cubic order, instead of the common quadratic form [1, 11]. For simplicity, we take the cubic term to be diagonal, and so

$$u(\vec{\rho}) = -\frac{v_2}{2} \sum_{i=1}^N \sum_{j=1}^N J_{ij} \rho_i \rho_j + \frac{v_3}{6} \sum_{i=1}^N \rho_i^3 N^2, \quad (3)$$

where $v_2 > 0$ and $v_3 > 0$ are constants that quantify the strength of the interactions and J_{ij} is the pairwise affinity matrix (the N^2 factor keeps the scale of the term proportional to v_3 independent of N for $\rho_i \sim N^{-1}$). Note that the quadratic term can be attractive ($J_{ij} > 0$) and

repulsive ($J_{ij} < 0$), whereas we only consider a repulsive cubic term. The role of the cubic term will become clear later.

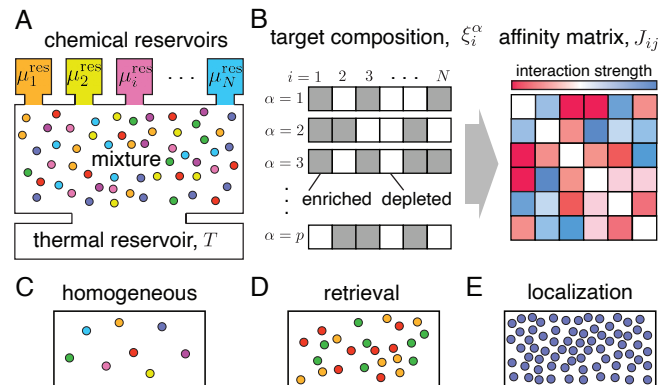


FIG. 1. *Schematic representation of the problem setup.* **A.** A liquid mixture with components $i = 1, \dots, N$ is in contact with a thermal reservoir at temperature T and chemical reservoirs with chemical potentials μ_i^{res} . **B.** Binary composition target vectors ξ_i^α indicate which components should be enriched or depleted in the retrieval states of interest. The p targets are used to design the affinity matrix, J_{ij} . **C-E.** Depending on the thermodynamic parameters, we distinguish three types of stable liquid states: homogeneous states, where all components mix equally; retrieval states, which are enriched/depleted according to the targets; and localised states, enriched in a small number of components.

To study metastable states of this mixture, we consider a setting in which the fluid is in contact with a thermal reservoir at temperature T and N chemical reservoirs at chemical potentials μ_i^{res} , see Fig. 1A. Hereafter, we assume for simplicity that all chemical potentials are equal, i.e., $\mu_i^{\text{res}} = \mu^{\text{res}}$. Metastable states are determined by densities $\vec{\rho}_*$ that satisfy the following two conditions.

The first condition is *chemical equilibrium*, by which the chemical potentials of the fluid, $\partial f / \partial \rho_i$, match those of the reservoir, i.e.,

$$\frac{\partial f}{\partial \rho_i}(\vec{\rho}_*) = \mu^{\text{res}}, \quad (4)$$

for all $i \in \{1, 2, \dots, N\}$.

The second condition is *mechanical stability*, i.e., the Hessian $H_{ij} = \partial^2 f / \partial \rho_i \partial \rho_j$ (inversely proportional to the isothermal compressibility [19]) is positive semi-definite,

$$\sum_{i=1}^N \sum_{j=1}^N H_{ij}^* x_i x_j \geq 0, \quad (5)$$

where $H_{ij}^* = H_{ij}(\vec{\rho}_*)$ and \vec{x} are arbitrary vectors in \mathbb{R}^N . The equality in (5) is attained when $\vec{\rho}_*$ is located at the *spinodal* manifold.

Defining the functional

$$\omega(\vec{\rho}, \mu^{\text{res}}) = f(\vec{\rho}) - \rho \mu^{\text{res}}, \quad (6)$$

which we call the *extended potential*, chemical equilibria are stationary points of ω w.r.t. $\vec{\rho}$ at fixed μ^{res} . Such points are mechanically stable when they are *local minima* of the extended potential. The grand potential of the fluid mixture is given by the value of ω evaluated at its global minimum.

II. METASTABLE TARGETS AND RETRIEVAL

We use the framework of Sec. I, to study the physical limitations on the stability of states with specified compositions. Our goal is to construct an affinity matrix J_{ij} , so that the liquid exhibits metastable states corresponding to p pre-defined *target* composition vectors ξ_i^α , with $\alpha = 1, \dots, p$. The *targets* have binary entries that determine whether component i should be enriched ($\xi_i^\alpha = 1$) or depleted ($\xi_i^\alpha = 0$), see Fig. 1A and B. We say that a fluid is then capable of retrieving the target state α if the corresponding metastable state is enriched as prescribed by ξ_i^α .

To endow the fluid with this retrieval capability, we draw inspiration from the classical work on neural networks by J.J. Hopfield [23] and propose as affinity matrix

$$J_{ij} = \sum_{\alpha,\beta=1}^p \gamma_i^\alpha c_{\alpha\beta}^{-1} \gamma_j^\beta, \quad (7)$$

where $\vec{\gamma}^\alpha = (\xi_i^\alpha - q)/n$, $c_{\alpha\beta} = \sum_{i=1}^N \gamma_i^\alpha \gamma_i^\beta / N$ is a covariance matrix, and $c_{\alpha\beta}^{-1}$ its inverse. Here, $q = Q/N$ is the sparsity parameter, equal for all targets, with Q the number of components enriched in the target compositions (i.e., for which $\xi_i^\alpha = 1$, see Fig. 1B), and $n = \sqrt{q(1-q)}$ is a normalization factor. Due to its combination of concepts from multi-components fluids and neural networks, we refer to this model as the *liquid Hopfield model*. Notice that for orthogonal $\vec{\gamma}^\alpha$ we recover

$$J_{ij} = \sum_{\alpha=1}^p \gamma_i^\alpha \gamma_j^\alpha, \quad (8)$$

which we recognize as the interaction matrix used by Hopfield in Ref. [18].

Our approach to study retrieval in the liquid Hopfield model is as follows. We first focus on a special set of targets, for which $\vec{\gamma}^\alpha$ are the columns of Sylvester-Hadamard matrices (see Appendix A). We call these the *hypersymmetric* targets. While a seemingly peculiar choice, we later show that hypersymmetric targets are the most stringent choice, i.e., when these targets are stable, then for the same model parameters any other set of targets are also stable. Therefore, we first focus on hypersymmetric targets in Secs III–VI, and then generalize our results for arbitrary targets in Secs. VII.

III. STATE STABILITY DIAGRAM

Figure 2 shows the stability diagram of the liquid Hopfield model for hypersymmetric targets. The Figure depicts the region where the homogeneous state of the mixture is stable (violet), the region where all p targets can be retrieved (green), and two regions where retrieval is not possible (orange). Boundaries of these regions are the *spinodal* lines of the corresponding states.

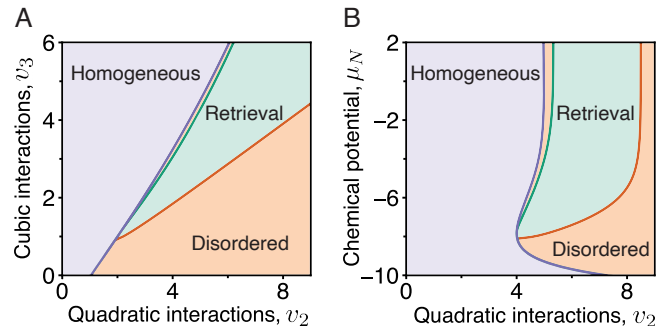


FIG. 2. *Stability diagrams for hypersymmetric targets.* **A.** Spinodal lines delimiting the regions where either the homogeneous state or all retrieval states are stable as a function of v_2 and v_3 with $\mu_N = -6$. The plotted lines are given by the equalities in Eqs. (10), (14) and (15). Note that retrieval only occurs for large enough cubic interactions v_3 . **B.** Same as Panel A, albeit as a function of v_2 and μ_N and with $v_3 = 4$. Note that retrieval only occurs for large enough chemical potential μ_N .

The stability of the homogeneous state for $v_2 \approx 0$ is expected, as in this regime contributions from entropy and cubic repulsion dominate, which mix all different components equally.

For sufficiently large repulsion, v_3 , retrieval of target compositions is possible, and corresponding *retrieval* states are stable. Between the homogeneous and retrieval region there is a small transition region. The retrieval region expands as v_2 and v_3 increase.

For v_2 large enough, stability of retrieval states is lost and the system enters a disordered region in which many different non-retrieval states are locally stable. For $v_2 \gg v_3$, states with few components, which we call *localized* states, are globally stable. As we clarify later on, since the cubic repulsive term penalizes such localized states, this elucidates the role of v_3 in stabilizing retrieval.

IV. HOMOGENEOUS REGION

A homogeneous state of the mixture has densities $\rho_i = \rho/N$ for all components i . The homogeneous states for hypersymmetric targets satisfy the condition of chemical equilibrium, given by Eq. (4), when $\rho = \rho_*$ with

$$\rho_* = \frac{1}{1 + \exp(-\mu_N + \frac{v_3}{2}\rho_*^2)}, \quad (9)$$

and where $\mu_N = \mu^{\text{res}} + \ln N$ is a rescaled chemical potential (see Appendix B). Note that in the limit $N \gg 1$ for fixed μ^{res} it holds that $\mu_N \gg 1$ and $\rho_* \rightarrow 1$, whereas for fixed μ_N we have that ρ_* is independent of N . In the following, we work on the second, arguably more physical, ensemble.

Now, we study the stability of the homogeneous state. Equation (5) holds if and only if all eigenvalues of the Hessian H_{ij} are non-negative. We therefore diagonalize H_{ij} at the homogeneous state analytically, see Appendix C. The non-negativity of the smallest eigenvalue yields the inequality

$$\rho_* (v_2 - v_3 \rho_*) \leq 1. \quad (10)$$

The equality in (10) is attained at the *spinodal* manifold, denoted by the violet lines in Fig. 2, for which the homogeneous state is marginally stable; in the low-temperature and dense limit, $v_2 \gg 1$ and $\mu_N \gg 1$, this reduces to $v_3 = v_2$. At the *spinodal* manifold, the unstable modes are spanned by the subspace of the target compositions $\vec{\gamma}^\alpha$. While this could be taken to suggest that the corresponding retrieval states are stable, see also analysis in [1, 13, 24, 25], we will later show that this is only the case in presence of cubic repulsion.

V. RETRIEVAL REGION

In the retrieval region, the mixture can adopt a stable density pattern according to a particular hypersymmetric target α . In particular, the density of component i is enriched when $\gamma_i^\alpha = 1$ and depleted when $\gamma_i^\alpha = -1$. Therefore, to characterize retrieval we use the *ansatz*

$$\rho_i^\alpha = \frac{\rho}{N} (1 + a \gamma_i^\alpha) \quad (11)$$

for retrieval states, where $a \in [-1, 1]$ measures the degree of retrieval, and which we call the *overlap* between the state of the mixture and the target state [23]. Imposing chemical equilibrium on this *ansatz* we find that retrieval states are chemically stable when $a = a_*$ and $\rho = \rho_*$ with

$$a_* = \tanh [a_* \rho_* (v_2 - v_3 \rho_*)], \quad (12)$$

$$\rho_* = \frac{1}{1 + \exp \left(-\mu_N + \frac{v_3}{2} \rho_*^2 (1 + a_*^2) + \frac{1}{2} \ln(1 - a_*^2) \right)}, \quad (13)$$

see Appendix B for a detailed derivation.

In Fig. 3A and B, we plot the solutions of (12) and (13) as a function of the quadratic interaction strength, v_2 , for different values of the rescaled chemical potential, μ_N . The figure shows that the retrieval state emerges from the homogeneous state at its spinodal line. We remark that due to the $a_* \rightarrow -a_*$ symmetry in (12) and (13) (consequence of $q = 1/2$) a second “mirror” state also emerges in which enrichment is opposite to that of the target α . Evaluating the extended potential $\omega(\vec{\rho})$ in

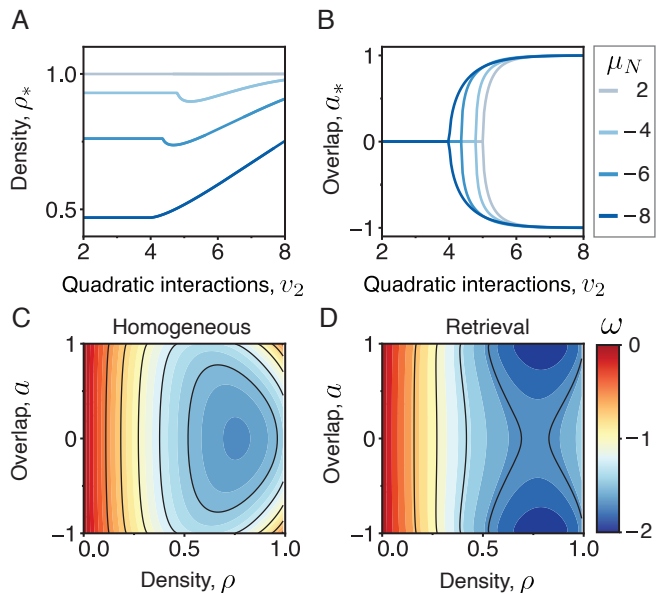


FIG. 3. *Chemical equilibrium of homogeneous and retrieval states.* **A.** The total density ρ_* as a function of the quadratic interaction strength v_2 for states in chemical equilibrium is shown for different values of the chemical potential μ_N [Eq. (13)]. **B.** Same as Panel A, but for the overlap a_* [Eq. (12)]. The overlap becomes non-zero outside the homogeneous region, indicating the emergence of the retrieval region. **C.** Heatmap of the extended potential ω evaluated at the retrieval ansatz (11) as a function of (a, ρ) for $v_2 = 2$, $\mu_N = -6$, and $v_3 = 4$. The minimum represents the homogeneous state. **D.** Same as Panel C but with $v_2 = 6$. In this case there are two mirror symmetric minima ($a \leftrightarrow -a$) that correspond to retrieval states.

the subspace spanned by Eq. 11 suggests that the retrieval state is not only a stationary point, but a stable minimum, see Fig. 3C and D. However, a complete stability picture requires studying the N -dimensional stability condition in (5), which we do in the following.

Deriving an analytical expression for the smallest eigenvalue of the Hessian (Appendix D), we find that a retrieval state is stable when the following two conditions hold

$$\rho_* (1 + a_*) (v_2 - v_3 \rho_* (1 + a_*)) \leq 1, \quad (14)$$

$$\rho_* (1 - a_*) (v_2 - v_3 \rho_* (1 - a_*)) \leq 1, \quad (15)$$

where (ρ_*, a_*) are taken from (12) and (13). The two equalities above correspond to the orange and green lines, respectively, of Fig. 2 when $a_* > 0$ (and the other way around when $a_* < 0$). The corresponding instability modes are confined into the space spanned by the target compositions. Note that between the homogeneous and retrieval regions there exists a narrow transition band. In the low-temperature and high density regime, the width of the transition region scales asymptotically as $\log(v_2)$, and the width of the retrieval region as $v_2/2$.

Two important facts can be deduced from (14) and

(15). First, in absence of the repulsive cubic interaction, i.e., $v_3 = 0$, adding the inequalities gives $\rho_* v_2 \leq 1$, which by Eq. (12) implies that $a_* = 0$, and so there are no retrieval states, see also Fig. 2. Therefore, sufficiently strong non-linear repulsion is necessary for retrieval. Second, Eq. (14) does not depend on the number of species N nor on the number of targets p . Consequently, the hypersymmetric liquid Hopfield model allows up to $N-1$ target compositions to be simultaneously stable, provided cubic repulsion is strong enough.

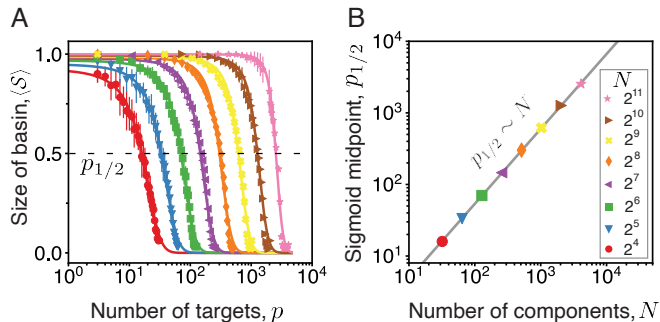


FIG. 4. *Scaling of basins of attraction of retrieval states* **A**. The mean size of the basin of attraction of retrieval states, $\langle S \rangle$, is plotted against the number of targets, p , for mixtures with different number of components, N . Sigmoidal curves are fit to each set of points. As the number of targets increases, the size of the basin of attraction shrinks. **B**. Scaling of the mid-point of each sigmoidal, $p_{1/2}$, as a function of the number of components in the mixture, N . A linear scaling is compatible with the observed trend (line corresponds to $p_{1/2} = (0.622 \pm 0.002)N - (11 \pm 3)$). In both panels, hypersymmetric targets are considered and the following parameters remain fixed: $\mu_N = 1$, $v_2 = 6$ and $v_3 = 4$. See Appendix H for a detailed description on the approach followed to produce this figure.

So far, we have shown that stability of retrieval states is independent on the number of components, N , and hypersymmetric targets, p . We now determine how the sizes of the basins of attraction depend on p and N . To this end, we quantify the size of a basin of attraction in terms of the number of component densities in an initial state that need to be set equal to corresponding values in the retrieval state of interest in order for a gradient descent dynamics in ω to converge to that retrieval state. We denote the associated observable as \mathcal{S} (see Appendix H for a definition).

Figure 4A, shows how the average size of the basins, $\langle S \rangle$, depends on the number of targets, p , for mixtures with different number of components, N . Basins decrease in size as p increases, as expected, and so retrieval is effectively more difficult as more targets are encoded. The mid-point of this decrease, $p_{1/2}$, measures the capacity of a liquid mixture to encode different target compositions. Interestingly, we find that this mid-point increases linearly with the number of components, N , see Figure 4B. This implies that as the number of components in a mixture increases, the number of states that can be re-

trieved increases proportionally. This scaling is reminiscent of the behavior of the capacity of associative neural networks [23].

VI. LOCALIZATION IN THE DISORDERED REGION

We now focus on the disordered region, where neither the homogeneous nor the retrieval states are stable. One of the key features of this region is that locally stable states overlap with multiple target compositions, yet they are enriched in a small fraction of components.

We first consider the analytically solvable case of $v_3 = 0$, $\mu = 0$, and $v_2 \gg 1$. In this case, states in which only one component is enriched, i.e., $\rho_i = \delta_{i,k}$ with $k \in \{1, 2, \dots, N\}$ fixed, are minima of the extended potential $\omega(\vec{\rho})$ located at the corners of the simplex. Furthermore, for large enough values of p these states are the only configurations that minimise ω , as shown in Appendix F. Corners of the simplex are fully localised states in the set of components, in the sense that they are enriched in only one component, and reminiscent of Anderson localisation for electrons in disordered materials [26, 27]. Therefore, for the case considered and p large, minima in the disordered region correspond to localized states.

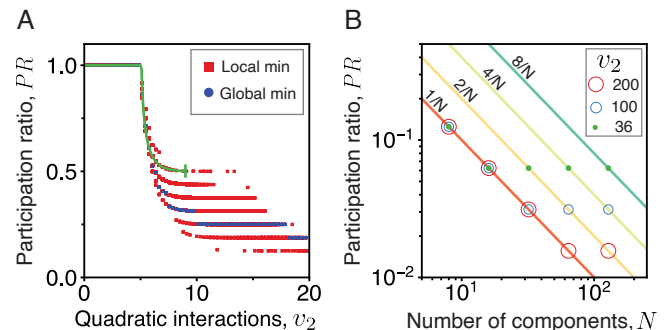


FIG. 5. *Non-retrieval and localization* **A**. Participation ratio, PR , of local and global minima of the extended potential ω as a function of the quadratic interaction strength, v_2 for $N = 32$, $p = 17$, $v_3 = 6$ and $\mu_N = 1$. The green line indicates the participation ratio $1/(1 + a_*^2)$ of the homogeneous and retrieval states. Observe how the PR gradually decreases as a function of v_2 which is a signature of localisation in the limit of large v_2 . **B**. Finite size scaling analysis of the participation ratio of the global minimum for given values of v_2 and with $p = 24$, $\mu_N = 1$, and $v_3 = 3$. Note that the saturation value at large N decreases as a function of v_2 . Markers represent the PR of states obtained from numerically minimizing the extended potential $\omega(\vec{\rho})$ for hypersymmetric targets, as explained in Appendix H.

More generally, localization is quantified by the *partic-*

icipation ratio

$$\text{PR}(\{\rho_i\}) = \frac{1}{N} \frac{\left(\sum_{i=1}^N \rho_i\right)^2}{\sum_{i=1}^N \rho_i^2}, \quad (16)$$

with $\lim_{N \rightarrow \infty} \text{PR}(\{\rho_i\}) > 0$ for a delocalised state, and $\lim_{N \rightarrow \infty} \text{PR}(\{\rho_i\}) = 0$ for a localised state. Figure 5A shows the participation ratio as a function of v_2 of minima of ω obtained numerically. For low v_2 , the homogeneous state is stable, and so $\text{PR} = 1$. At intermediate v_2 , the retrieval state becomes stable, for which $\text{PR} = 1/(1 + a_*^2)$. In addition, we also observe other non-retrieval states that are locally stable, which are reminiscent of spurious states in associative neural networks [23]. For large values of v_2 , these non-retrieval states have a decreasing PR, with the discrete jumps observed corresponding to the full depletion of components one by one.

We further studied the role of increasing the number of components on localization. Fig. 5B shows that the PR saturates to a constant value as N increases. This asymptotic value decreases as a function of the quadratic interaction, v_2 , and the number of targets, p , see Appendix F. Therefore, stable states are localized for $v_2 \gg 1$ and an extensive number of targets $p \sim N$, in agreement with the analytical results at the beginning of this section.

Taken together, stable states in the disordered region have a small PR and localize in the limit of v_2 large and many targets $p \sim N$. This supports the idea that stability of the retrieval region is related to the suppression of localization.

VII. GENERALIZATION TO ANY TYPE OF TARGETS

Up until now, we have restricted our study to the case of hypersymmetric targets. We now generalize the results to completely generic targets. First, we will discuss the case of $q = 1/2$, for which the stability diagram appears in Fig. 6.

For generic targets, the characteristics of the homogeneous state remain unchanged, so that Eqs.(9) and (10) apply (see Appendix C). Furthermore, the chemical equilibrium condition of the retrieval states is also valid, and so Eqs. (12) and (13) generalize to generic targets (see Appendix B). Moreover, for generic targets the retrieval region is larger than for hypersymmetric targets, and thus the latter represent a worse-case-scenario for retrieval. In particular, in Appendix D we mathematically prove that the conditions in Eqs. (14) and (15) are sufficient conditions for retrieval. Therefore, retrieval is stable in a region at least as large as in the case of hypersymmetric targets.

Beyond this, we find that each retrieval state has a distinctive *spinodal* line. This results in a new region of parameters for which only some of the retrieval states

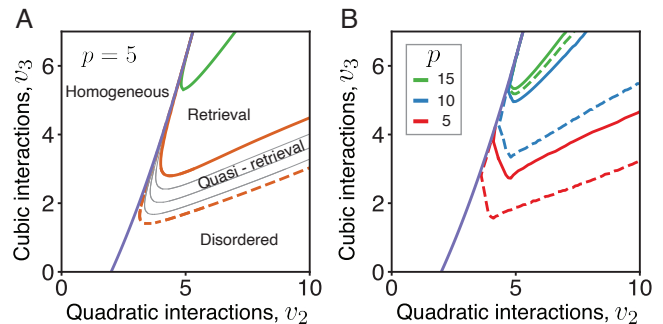


FIG. 6. *Stability diagrams for generic targets and $q = 1/2$.* **A.** Spinodal lines delimiting the regions where the homogeneous state or each of the $p = 5$ retrieval states are stable as a function of v_2 and v_3 . Note that there are p distinct spinodal lines, one for each of the target states, which yields the quasi-retrieval region. The stability line of retrieval for hypersymmetric targets is shown in green. **B.** Stability diagrams for different number of target states p . Lines are obtained by averaging the spinodal lines at each value of v_3 for fifty sets of targets independently generated. The solid and dashed lines of each color delimit the retrieval and quasi-retrieval region for the corresponding p . As p increases, lines delimiting the quasi-retrieval and retrieval region collapse on the retrieval spinodal for hypersymmetric targets. Targets have been generated through a random permutation of a vector with $q = 1/2$. Parameters are fixed for both panels to $\mu_N = 0$ and $N = 32$. Spinodal lines for generic targets are obtained numerically by diagonalizing the hessian at states in chemical equilibrium, see Eqs. (B4-B5)

are stable, which we term *quasi-retrieval*, see Fig. 6A. Interestingly, Fig. 6B reveals that as the number of targets increases the quasi-retrieval region gradually decreases in size until it coincides with the *spinodal* line of hypersymmetric targets, see Appendix D for a proof. Hence, for a large number of targets p , we recover the worse-case-scenario for hypersymmetric targets.

VIII. EFFECT OF SPARSITY ON RETRIEVAL

So far, we have restricted our study to generic targets for which $q = 1/2$. In this case half of the components are present in each target. We now consider the case of lower values of q , where less components are shared among targets.

Fig. 7A shows the region where the homogeneous state is stable and regions where all retrieval states are also stable for different values of the sparsity, q . Note that the spinodal for the homogeneous state, which we derive analytically in Appendix C, is independent of the sparsity q of the target states. In contrast with the homogeneous state, we find that stability of target states depends on the sparsity, and in fact reducing q , results in a larger retrieval region, consistent with previous results on multifarious self-assembly [3] and classical results of neural networks [28]. Specifically, the lines plotted in Fig. 7A

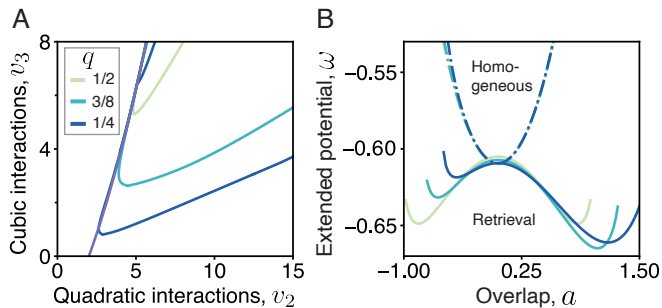


FIG. 7. *Stability diagrams for targets with variable sparsity.* **A.** Lines delimit the region where the homogeneous state is stable and the regions where all possible retrieval states with a given q are stable [see Eqs. (D14) and (D15) in Appendix D]. Parameters chosen are $p = 25$, $N = 32$, and $\mu_N = 0$. **B.** The extended potential ω evaluated at the retrieval ansatz (11) with $\rho = \rho_*$ is plotted as a function of the overlap a , where ρ_* solves Eq. (B5) for a given a . Different colours correspond with varying values of the sparsity q . The single-well potential corresponds to the homogeneous regime $v_2 = 2$ and the double-well potential to the retrieval $v_2 = 8.5$. Other parameters chosen are $v_3 = 4$, $\mu_N = 0$. Notice that in the retrieval region the mirror symmetry $a \rightarrow -a$ is broken for $q \neq 1/2$.

represent the worse case scenario for the stability of target states in the large p limit, and we derive those analytically in Appendix B. Interestingly, we find that the key result that nonlinearities are necessary for retrieval, i.e. retrieval requires $v_3 \neq 0$, still hold even in the limit $q \rightarrow 0$, as shown in Appendix G.

Recall that for $q = 1/2$ each target state came accompanied by a mirror state for which $a_* < 0$. Changing the sparsity of the targets from $q = 1/2$ breaks the symmetry $a_* \rightarrow -a_*$ in the corresponding equations. As a consequence, the values of the extended potential for the mirror states increases as q decreases, see Fig. 7B. Hence, the case of low q thermodynamically suppresses mirror states, as desired.

Taken together, this shows that sparse targets facilitate retrieval, by increasing the parameter region where retrieval is stable and by suppressing potentially undesired mirror states.

IX. DISCUSSION

A. Summary

Biological mixtures often consist of a large number of different components [8, 29–32]. Despite this, such mixtures are not disordered, but instead assemble into functional states with well characterized composition. Resolving this apparent paradox is challenging because there is no established physics formalism to describe materials with such characteristics.

In this paper, we have introduced the liquid Hopfield model as a simple paradigm for multi-component mixtures capable of retrieving multiple target compositions. Our analysis revealed a trade-off between retrieval of targets states, related to functional biological states; and disordered localized states, in which only few components are enriched. Such trade-off is controlled by repulsive non-linear interactions, which can be interpreted as a higher order term in the virial expansion of the free energy. Taken together, our results shed light on the relation between localisation and the retrieval capability of complex mixtures.

B. Relationship to previous work

The liquid Hopfield model belongs to a family of classical statistical physics models for multicomponent mixtures, $N \gg 1$, that rely on free energies of the form described in Sec. I, see references in the introduction. The present paper establishes an expression for the pairwise interactions, J_{ij} , as a function of the desired target compositions, $\vec{\xi}^\alpha$. This expression guarantees stability of up to $p = N - 1$ arbitrary targets enriched in any number of components Q . We have thus provided an explicit solution to the inverse problem investigated numerically in [16, 17], where however stability was only guaranteed for p substantially smaller than N with an important dependence on Q . Furthermore, while previous work focused on specific parameter choices, in the present work we analytically determined the parameter regions where retrieval is possible.

Besides recent work on fluids, the liquid Hopfield model is also related to earlier models for *multifarious* self-assembly of solid structures [3, 10]. The main difference is that the interactions in [3, 10] are specific to reflect the spatial geometry of assemblies, whereas in this work interactions are non-specific, which results in more cross-talk.

Such cross-talk translates in the emergence of disorder at low temperatures. Finding the minimal configurations of the free energy (1-3) at zero temperature is then equivalent to solving a quadratic programming problem. For a general choice of J_{ij} this is an NP-hard problem [33–35], which implies a rugged low-temperature free-energy landscape akin to a spin glass phase [36, 37]. In spite of this challenge, numerical and analytical results in this paper show that at low temperatures stable states are indeed disordered and tend to localize, i.e., are enriched in few components, consistent with results from simulations [11, 12].

The tendency for disorder that emerges from cross-talk results in a trade-off between states that retrieve target compositions and disordered localised states. In fact, nonlinear repulsion is necessary to confine the densities away from the boundaries of the simplex and thus suppress localization and enable retrieval. We remark that such confining non-linearity is needed despite the pres-

ence of nonlinear entropic terms, which are sufficient to provide chemical stability, but not mechanical stability, unlike for binary mixtures. The need for “strong” nonlinearities is in agreement with results of neural network models for continuous neuronal activity. In fact, the classic continuous implementation of J.J. Hopfield [38] required a strong sigmoidal nonlinearity for retrieval. Non-linearities are also key in more modern variants of Hopfield networks with continuous variables [39–41], which require a quartic term in the energy functional for successful retrieval. For the above reasons, we expect that the requirement of a nonlinear term is a generic requirement for retrieval in multi-component mixtures with structured interactions.

C. Perspective

The results we presented open many natural avenues of future research. Within the specific context of the model, we highlight three. First, it remains open how the key results extend to the canonical ensemble, which may be achieved following a similar analytical approach under a different *ansatz*. Second, the potential role of dissipation, e.g., in stabilizing target phases, remains unaddressed. Third, while we assumed a particular set of interactions, we have not addressed how a mixture can acquire these interactions. Clearly, protein affinities are not random, but have instead evolved to comply with a particular function [3, 16]. It remains to be seen whether evolutionary dynamics can parsimoniously converge to the affinity matrix here proposed, recapitulating the success of neuronal learning rules [23].

Besides these theoretical implications, we also foresee experimental implications. Although the liquid Hopfield model constitutes a simple paradigm for cytoplasmic aggregates often referred to as liquid droplets, it is yet to be shown that its key findings are in agreement with properties of such cellular structures. Besides this, it is also possible that synthetic experimental constructs of liquid mixtures may be engineered to recapitulate such key findings, as it has recently been attempted for multifarious assembly models using DNA origami [42].

More generally, this work is the first to establish a direct relationship between the theory of neural computation and that of multi-component liquid mixtures (for solid assemblies, a similar path was followed in [3, 10]). Given the vibrant recent advances in both areas, this work suggests that different aspects of neural computation may be applied to liquid mixtures. Examples of these are classical information processing capabilities of feed-forward neural networks, e.g. classification, or dynamic properties such as sequential retrieval [23].

ACKNOWLEDGMENTS

GC is supported by the EPSRC Centre for Doctoral Training in Cross-Disciplinary Approaches to Non-Equilibrium Systems (CANES, EP/L015854/1). RBT acknowledges financial support from the Portuguese Foundation for Science and Technology (FCT) under the contract 2022.12272.BD. PS was partly funded by a grant from laCaixa (LCF/BQ/PI21/11830032).

Appendix A: Hypersymmetric targets

We define the hypersymmetric targets $\vec{\gamma}^\alpha$. These target vectors are the columns of Sylvester-Hadamard matrices of order $M = 2^k$, $\mathcal{H}(k)$ [43], and hence we first define the Sylvester-Hadamard matrices. These matrices are constructed through the following iteration,

$$\mathcal{H}(1) = \begin{bmatrix} 1 & 1 \\ 1 & -1 \end{bmatrix} \Rightarrow \mathcal{H}(k) = \begin{bmatrix} \mathcal{H}(k-1) & \mathcal{H}(k-1) \\ \mathcal{H}(k-1) & -\mathcal{H}(k-1) \end{bmatrix}, \quad (\text{A1})$$

which results in the first column having all components equal to one. Hereafter we do not explicitly indicate k specifying the order 2^k of the matrices.

Importantly, the columns of these matrices form a Boolean group. In particular, for any two columns u and v with matrix entries \mathcal{H}_{iu} and \mathcal{H}_{iv} , there exists a third column w such that

$$\mathcal{H}_{iw} = \mathcal{H}_{iu}\mathcal{H}_{iv}. \quad (\text{A2})$$

This follows from the fact that

$$\mathcal{H}_{iu} = (-1)^{\sum_{\ell=1}^k n_\ell^{(i)} n_\ell^{(u)}}, \quad (\text{A3})$$

where $n_\ell^{(i)}$ are the digits of i when it is written in the base-2 numeral system, i.e., $i = \sum_{\ell=1}^k n_\ell^{(i)} 2^{\ell-1}$.

We can now define the hypersymmetric targets. For $p = M - 1$, the targets are the columns of Sylvester-Hadamard matrices, excluding the first column $u = 1$, i.e. $\gamma_i^\alpha = \mathcal{H}_{iu}$. For $p < M - 1$, the targets are chosen randomly among the columns $u > 1$ of Sylvester-Hadamard matrices ensuring that for each target state $\vec{\gamma}^\alpha$ there exists two target states $\vec{\gamma}^{(\beta_1)}$ and $\vec{\gamma}^{(\beta_2)}$ such that (A2) is satisfied, that is:

$$\gamma_i^\alpha = \gamma_i^{(\beta_1)} \gamma_i^{(\beta_2)}. \quad (\text{A4})$$

This condition (A4) is required to recover the worst-cases scenario, i.e., if the retrieval state is stable for those targets, than it is stable for any other set of targets.

For $p > M/2$, the condition (A4) is satisfied for all combinations of p targets. Indeed, this can be proven through contradiction. Assume that there exists one target state, say $\vec{\gamma}^\alpha$, for which there exist no two other target states $\vec{\gamma}^{(\beta_1)}$ and $\vec{\gamma}^{(\beta_2)}$ such that (A4) holds. In this case, we can construct the $p-1$ vectors with entries $\zeta_i^\beta = \gamma_i^\alpha \gamma_i^\beta$ where $\beta \neq \alpha$, which by assumption are not target states. However, since the columns of the Hadamard matrix form a group under the element wise product, the $\vec{\zeta}^\beta$, with $\beta \neq \alpha$, are $p-1$ distinct columns of the Hadamard matrix. Hence, within our assumptions, the $p-1$ vectors $\vec{\zeta}^\beta$ with $\beta \neq \alpha$, the $p-1$ target states $\vec{\gamma}^\beta$ with $\beta \neq \alpha$, the target state $\vec{\gamma}^\alpha$, and the all-ones vector, should all be distinct columns of the Hadamard matrix. However, this is not possible as we count $2p > M$ vectors and the Hadamard matrix has by construction only M columns.

Appendix B: Chemical equilibrium for homogeneous and retrieval states

In this Appendix, we derive the conditions under which the *ansatz* in Eq. (11) is in chemical equilibrium. We derive these conditions for affinity matrices of the form (7), and these conditions reduce to (9) for $a_* = 0$ and to Eqs. (12) and (13) for $q = 1/2$.

The condition for chemical equilibrium in Eq. (4) can be written explicitly as

$$-v_2 \sum_{j=1}^N J_{ij} \rho_j + \frac{v_3}{2} \rho_i^2 N^2 + \log \rho_i = \log(1 - \rho) + \mu^{\text{res}}, \quad (\text{B1})$$

which yields N coupled equations. Substituting the retrieval *ansatz* given by Eq. (11) into (B1) gives

$$\begin{aligned} & -v_2 \sum_{j=1}^N J_{ij} \frac{\rho_*}{N} (1 + a_* \gamma_j^\alpha) + \frac{v_3}{2} \rho_*^2 (1 + a_* \gamma_i^\alpha)^2 \\ & + \log \frac{\rho_* (1 + a_* \gamma_i^\alpha)}{N} = \log(1 - \rho_*) + \mu^{\text{res}}. \end{aligned} \quad (\text{B2})$$

We now use two properties of the affinity matrix J_{ij} of Eq. (7): first, the all-ones vector belongs to the kernel of J_{ij} ; and second, the target vectors, $\vec{\gamma}^\alpha$, are eigenvectors of J_{ij} with eigenvalue N . From this, we can simplify Eq. (B2) into

$$\begin{aligned} & -v_2 \rho_* a_* \gamma_i^\alpha + \frac{v_3}{2} \rho_*^2 (1 + a_* \gamma_i^\alpha)^2 + \log \frac{\rho_* (1 + a_* \gamma_i^\alpha)}{N} \\ & = \log(1 - \rho_*) + \mu^{\text{res}}. \end{aligned} \quad (\text{B3})$$

Note that because the targets are binary, this reduces the N stability equations to two equations: one for $\gamma_i^\alpha = (1 - q)/n$ and the other one for $\gamma_i^\alpha = -q/n$. Solving these towards a and ρ we get the chemical equilibrium conditions for target states with arbitrary q :

$$\begin{aligned} a_* &= n \frac{\exp(w) - 1}{1 - q + q \exp(w)}, \\ \frac{1}{\rho_*} &= 1 + \exp \left[-\mu_N + \frac{1}{2} v_3 \rho_*^2 (1 + a_*^2) \right. \\ & \quad \left. + q \log \left(1 + a_* \frac{1 - q}{n} \right) + (1 - q) \log \left(1 - a_* \frac{q}{n} \right) \right], \end{aligned} \quad (\text{B4})$$

where $w = \frac{1}{n} [v_2 \rho_* a_* - \frac{1}{2} v_3 \rho_*^2 (2a_* + a_*^2 \frac{1-2q}{n})]$ and $n = \sqrt{q(1-q)}$. Equations (B4) and (B5) reduce to Eq. (9) in the particular case of $a_* = 0$, and to Eqs. (12) and (13) for $q = 1/2$.

Appendix C: Exact diagonalization of the Hessian in homogeneous state

We diagonalize the Hessian in a homogeneous state $\rho_i = \rho/N$, which takes the form

$$H_{ij} = -v_2 J_{ij} + \frac{1}{1-\rho} + \delta_{ij} \left(\frac{N}{\rho} + v_3 N \rho \right), \quad (\text{C1})$$

where J_{ij} is given by Eq. (7).

The spectrum of this matrix consists of three eigenvalues, which we denote by λ_{ret} , λ_{cond} and λ_{\perp} . The retrieval eigenvalue is

$$\lambda_{\text{ret}} = \frac{N}{\rho} + v_3 N \rho - v_2 N. \quad (\text{C2})$$

Its eigenspace is a p -dimensional vector space spanned by the p targets $\bar{\gamma}^\alpha$ to be retrieved. The condensation eigenvalue is

$$\lambda_{\text{cond}} = \frac{N}{\rho} + v_3 N \rho + \frac{N}{1-\rho}, \quad (\text{C3})$$

and its corresponding eigenvector is the all-ones vector. The remaining eigenvalue is

$$\lambda_{\perp} = \frac{N}{\rho} + v_3 N \rho, \quad (\text{C4})$$

and has a $N - p - 1$ dimensional eigenspace that is orthogonal to the targets and the all-ones vector.

Since only λ_{ret} can be negative, the homogeneous state destabilises in a direction that is a linear combination of the target vectors. The condition in Eq. (10) for mechanical equilibrium is obtained by setting $\rho = \rho_*$ in the equation $\lambda_{\text{ret}} = 0$.

Appendix D: Lower bounds for eigenvalues of the Hessian in the retrieval state

Unlike in the homogeneous case, discussed in appendix C, we do not determine the full spectrum of the hessian in retrieval states. Nevertheless, we derive a lower bound for the eigenvalues of the Hessian which provide sufficient conditions for retrieval. Note that the lower bound applies to a generic set of p target vectors $\bar{\gamma}^\alpha$. Furthermore, we also show that for hypersymmetric targets, as defined in A, these conditions are in fact also necessary, which proves Eq. (14).

Substituting the retrieval ansatz (11) into the Hessian, $H_{ij} = \partial^2 f / \partial \rho_i \partial \rho_j$, we get the matrix

$$H_{ij}^\alpha = -v_2 J_{ij} + \frac{1}{1-\rho} + N \delta_{i,j} \left[v_3 \rho (1 + a \gamma_i^\alpha) + \frac{1}{\rho} \frac{1}{1 + a \gamma_i^\alpha} \right]. \quad (\text{D1})$$

Substituting $\gamma_i^\alpha = (\xi_i^\alpha - q)/n$, and using that $\xi_i^\alpha \in \{0, 1\}$, we get

$$H_{ij}^\alpha = -v_2 J_{ij} + \frac{1}{1-\rho} + N \delta_{i,j} (c_1 - c_2 \xi_i^\alpha), \quad (\text{D2})$$

where

$$c_1 = v_3 \rho (1 - a q/n) + \frac{1}{\rho} \frac{1}{1 - a q/n}, \quad (\text{D3})$$

and

$$c_2 = -\frac{v_3 \rho a}{n} + \frac{a}{n \rho} \frac{1}{(1 + a(1 - q)/n)(1 - a q/n)}. \quad (\text{D4})$$

Since the matrix H_{ij}^α is symmetric, its minimal eigenvalue $\lambda_{\text{min}}^\alpha$ can be obtained by solving the constrained minimization problem

$$\lambda_{\text{min}}^\alpha = \min_{\|\bar{x}\|=1} \left(\sum_{i=1}^N \sum_{j=1}^N x_i H_{ij}^\alpha x_j \right), \quad (\text{D5})$$

where

$$\begin{aligned} & \sum_{i=1}^N \sum_{j=1}^N x_i H_{ij}^\alpha x_j \\ &= -v_2 \sum_{i=1}^N \sum_{j=1}^N x_i J_{ij} x_j + \frac{1}{1-\rho} \left(\sum_{i=1}^N x_i \right)^2 \\ & \quad + N c_1 \sum_{i=1}^N x_i^2 - N c_2 \sum_{i=1}^N x_i^2 \xi_i^\alpha. \end{aligned} \quad (\text{D6})$$

Next, we bound $\lambda_{\text{min}}^\alpha$ from below by bounding the four terms in Eq. (D6):

- *interaction* term: since the affinity matrix J_{ij} in Eq. 7 has two eigenvalues, namely 0 and N , it holds that

$$-v_2 \sum_{i=1}^N \sum_{j=1}^N J_{ij} x_i x_j \geq -v_2 N \sum_{i=1}^N x_i^2 = -v_2 N. \quad (\text{D7})$$

- *entropic* term: this term is non-negative, and so

$$\frac{1}{1-\rho} \left(\sum_{i=1}^N x_i \right)^2 \geq 0. \quad (\text{D8})$$

- c_1 -term: as the norm of $\{x_i\}$ equals one, this term is constant,

$$N c_1 \sum_{i=1}^N x_i^2 = N c_1. \quad (\text{D9})$$

- c_2 -term: depending on the sign of c_2 we get different bounds. If $c_2 > 0$, then

$$-Nc_2 \sum_{i=1}^N x_i^2 \xi_i^\alpha \geq -Nc_2. \quad (\text{D10})$$

On the other hand, if $c_2 < 0$, then

$$-Nc_2 \sum_{i=1}^N x_i^2 \xi_i^\alpha \geq 0. \quad (\text{D11})$$

Adding the lower bounds for the individual terms, we get for $c_2 > 0$ that

$$\frac{\lambda_{\min}^\alpha}{N} \geq -v_2 + c_1 - c_2, \quad (\text{D12})$$

and for $c_2 < 0$,

$$\frac{\lambda_{\min}^\alpha}{N} \geq -v_2 + c_1. \quad (\text{D13})$$

The inequalities above can be used to derive sufficient conditions for retrieval, that is conditions on the parameters $\{v_2, v_3, \mu, q\}$ that, when satisfied, ensure stability of the retrieval states (but there may be other regions of parameters where retrieval is also stable). To do so, we set $a = a_*$ and $\rho = \rho_*$, where a_* and ρ_* solve Eq. (B3) ensuring chemical stability, and then we impose that the right-hand-side (RHS) of Eqs. (D12) and (D13) are greater or equal than zero. Since positivity of the RHS ensures $\lambda_{\min}^\alpha \geq 0$ we find the following sufficient conditions for stability of retrieval states,

$$-v_2 + c_1 - c_2 \geq 0 \quad (\text{D14})$$

for $c_2 > 0$, and

$$-v_2 + c_1 \geq 0 \quad (\text{D15})$$

for $c_2 < 0$. Note that if $c_2 > 0$, then (D14) implies (D15), and if $c_2 < 0$, then (D15) implies (D14). Hence, we can state mechanical stability conditions more simply as the requirement that both (D14) and (D15) are satisfied, without reference to c_2 . Remarkably, the sufficient conditions (D14) and (D15) for retrieval do not depend on p . Eqs. (D14) and (D15) were used in Fig. 6A to outline the boundary of the retrieval phase with arbitrary sparsity q .

For hypersymmetric targets, as defined in Appendix A, the inequalities in Eqs. (D12) and (D13) saturate. This implies that the conditions Eqs. (D14) and (D15) evaluated for $q = 1/2$ and $n = \sqrt{q(1-q)} = 1/2$ (corresponding with Eqs. (14) and (15) are both necessary and sufficient conditions for the stability of retrieval states with hypersymmetric targets. To show that the equality in Eq. (D12) is attained when the target vectors are hypersymmetric, we evaluate the quadratic function in Eq. (D6) at

$$\vec{x} = \frac{1}{\sqrt{2N}} \left(\vec{\gamma}^{(\beta_1)} + \vec{\gamma}^{(\beta_2)} \right). \quad (\text{D16})$$

Using the property Eq. (A4) that holds for hypersymmetric target vectors, we find that this choice of \vec{x} saturates Eq. (D12). For $c_2 < 0$ we obtain saturation using the vector

$$\vec{x} = \frac{1}{\sqrt{2N}} \left(\vec{\gamma}^{(\beta_1)} - \vec{\gamma}^{(\beta_2)} \right). \quad (\text{D17})$$

Appendix E: Collapse of the retrieval lines in the limit of large p and $q = 1/2$

Asides from the symmetric case, the inequalities in Eqs. (D12) and (D13) saturate in the limit of a large number of targets p . We observed this numerically for all values of q , and below we provide an analytical derivation for the case $q = 1/2$, which explains why in Fig. 6A the spinodal lines are determined by the equalities in Eq. (14) for large p .

To prove saturation at large values of p , we note that the equalities in (D14) and (D15) are attained for the vectors (D16) and (D17) because (i) \vec{x} is an eigenvector of J_{ij} ; (ii) \vec{x} is a linear combination of the two vectors $\vec{\gamma}^{(\beta_1)}$ and $\vec{\gamma}^{(\beta_2)}$ for which it holds that $\gamma_i^{(\beta_1)} \gamma_i^{(\beta_2)} = \gamma_i^\alpha$ for all i .

Here, we follow a similar approach. We evaluate the quadratic form in Eq. (D6) at the vector

$$\vec{x}^{(+,\alpha)} = \frac{1}{\sqrt{2N}} \left(\vec{\zeta}^{(\beta_1)} + \vec{\zeta}^{(\beta_2)} \right) \quad (\text{E1})$$

where $\vec{\zeta}^{(\beta_1)}$ and $\vec{\zeta}^{(\beta_2)}$ are two vectors, not necessarily target states, with entries $\zeta_i^{(\beta_1)}, \zeta_i^{(\beta_2)} \in \{-1, 1\}$, for which $\sum_i \zeta_i^{(\beta_1)} = \sum_i \zeta_i^{(\beta_2)} = 0$, and with $\zeta_i^{(\beta_1)} \zeta_i^{(\beta_2)} = \gamma_i^\alpha$. Such two states can be constructed as follows. First, we select a state $\vec{\zeta}^{(\beta_1)}$ with binary entries that is orthogonal to $\vec{\gamma}^\alpha$ and to the all ones vector. Second, we define the vector with entries $\zeta_i^{(\beta_2)} = \zeta_i^{(\beta_1)} \gamma_i^\alpha$. Since $p = N - 1$, it holds that the affinity matrix $J_{ij} = \delta_{i,j} - 1$, and therefore $\vec{x}^{(+,\alpha)}$ is an eigenvector of J_{ij} . Consequently, the inequality (D14) is saturated for when setting $\vec{x} = \vec{x}^{(+,\alpha)}$ in the quadratic form (D6). Analogously, we can consider a vector $\vec{x}^{(-,\alpha)}$ to obtain the second spinodal line (D15).

Appendix F: Equilibrium states at zero temperature

We now use a probabilistic argument to show that for $p > \log(N)/\log(2)$ the minima of the functional, ω Eq.6 in the limit of zero temperature, are the corners of the simplex of physical states. First, note that in the limit of $v_3 = 0$, $\mu^{\text{res}} = 0$, and $v_2 \gg 1$ the functional takes the quadratic form

$$\omega(\vec{\rho}, 0) = -\frac{v_2}{2} \sum_{i,j=1}^N J_{ij} \rho_i \rho_j. \quad (\text{F1})$$

Minimising a quadratic function over a simplex is an NP-hard problem called the quadratic concave optimization problem, see Refs. [33–35]. However, for the specific choice of J_{ij} in Eq. (7) it holds that

$$\omega(\vec{\rho}, 0) = -\frac{v_2}{2}\rho^2 \sum_{\alpha=1}^p m_\alpha^2, \quad (\text{F2})$$

where $m_\alpha = \sum_{i=1}^N \gamma_i^\alpha \rho_i$. The minima must have $\rho = 1$ and $m_\alpha = \pm 1$ for all values of α . Hence, the minima are obtained as solutions to equations of the form $m_\alpha = \sigma_\alpha$, with $\alpha \in \{1, 2, \dots, p\}$, and $\sigma_\alpha \in \{-1, 1\}$. The values of σ_α determine the corner on which we focus. We discuss the case of $\sigma_\alpha = 1$ for all α , but the other cases can be treated equivalently. The effect of each equation is to set $\rho_i^\alpha = 0$ whenever $\gamma_i^\alpha \neq 1$. In this way, given a set of p targets, a noncorner solution exists whenever there exist two or more components, say i and j , for which it holds that $\gamma_i^\alpha = \gamma_j^\alpha = 1$ for all $\alpha \in \{1, 2, \dots, p\}$. That is, whenever two or more components are shared by all targets. If the p targets are randomly selected, the probability that at least two components are shared in all targets is

$$p_{++} = \binom{N}{2} \frac{1}{2^{2p}} \quad (\text{F3})$$

where the first term counts the number of ways of selecting two components out of the N , and the second corresponds to the probability that both components are present in all p targets. We are interested in the behavior of p_{++} when $p, N \rightarrow \infty$. In this limit, we can write $p_{++} \approx \exp(-\zeta)$ with $\zeta = -2 \log(N) + 2p \log(2)$. Calculating when this probability approaches zero, determines when the minima of the functional are exclusively corners. We find that this occurs for $p > \log(N)/\log(2)$, as initially claimed.

Appendix G: Limit of sparse targets $q \rightarrow 0$

We discuss chemical and mechanical equilibrium conditions for retrieval states in the limit of $q \approx 0$ and for $v_3 \approx 0$. The main finding of this Appendix is that also in the sparse limit of $q = 0$ a finite $v_3 > 0$ is required to stabilize retrieval states. An analogous analysis applies for $q \approx 1$.

1. Chemical equilibrium

To take the limits $q \rightarrow 0$ and $v_3 \rightarrow 0$, we make the substitution

$$\hat{a}_* = \frac{a_*}{\sqrt{q}}, \quad (\text{G1})$$

in Eqs. (B4) and (B5), and consider the expansions

$$\hat{a}_* = \hat{a}_*^{(0)} + v_3 \hat{a}_*^{(1)} + O(v_3^2) \quad (\text{G2})$$

and

$$\rho_* = \rho_*^{(0)} + v_3 \rho_*^{(1)} + O(v_3^2). \quad (\text{G3})$$

Solving the resultant equations towards the densities we get the coefficients

$$\rho_*^{(0)} = \frac{1}{1 + e^{-\mu_N}} \quad (\text{G4})$$

and

$$\rho_*^{(1)} = -\frac{e^{-\mu_N}}{2(1 + e^{-\mu_N})^4}. \quad (\text{G5})$$

Note that in the limit of sparse target states, the densities do not depend on the overlap \hat{a}_* , and hence retrieval regions are enriched in a few components, but their overall density will not differ from the exterior density. Also, note that the correction term $\rho_*^{(1)}$ is negative as v_3 quantifies the strength of a repulsive potential.

For the coefficients of the overlap parameter, we obtain the implicit equation

$$\hat{a}_*^{(0)} = \exp(\hat{a}_*^{(0)} \hat{v}_2) - 1, \quad (\text{G6})$$

where $\hat{v}_2 = v_2/(1 + e^{-\mu_N})$. Apart from the trivial solution $\hat{a}_*^{(0)} = 0$, Eq. (G6) admits the solution

$$\hat{a}_*^{(0)} = \begin{cases} -1 - \frac{1}{\hat{v}_2} W_{-1}(-e^{-\hat{v}_2} \hat{v}_2) & \text{if } \hat{v}_2 \leq 1, \\ -1 - \frac{1}{\hat{v}_2} W_0(-e^{-\hat{v}_2} \hat{v}_2) & \text{if } \hat{v}_2 > 1, \end{cases} \quad (\text{G7})$$

where $W_0(x)$ is the principal branch of the Lambert-W function that solves $x = W e^W$, and $W_{-1}(x)$ is the second branch of the Lambert-W function. The coefficient for the linear term in perturbation theory is given by

$$\hat{a}_*^{(1)} = \hat{a}_*^{(0)} \frac{e^{-\mu_N + \hat{a}_*^{(0)} \hat{v}_2}}{2(1 + e^{-\mu_N})^4} \times \frac{4 + 2\hat{a}_*^{(0)} + v_2 + 2(2 + \hat{a}_*^{(0)}) \cosh(\mu_N)}{(-1 + \hat{v}_2 e^{\hat{a}_*^{(0)} \hat{v}_2})}. \quad (\text{G8})$$

Note that when $\hat{a}_*^{(0)} = 0$, $\hat{a}_*^{(1)}$ is in general not zero-valued, as the denominator also converges to zero in this limit, yielding a finite value for $\hat{a}_*^{(1)}$.

In Fig. 8 we plot \hat{a}_* as a function of \hat{v}_2 up to linear order in perturbation theory. Observe that $\hat{a}_*^{(0)}$ is positive for $\hat{v}_2 < 1$ and negative for $\hat{v}_2 > 1$, while for $v_3 > 0$ the transition point where \hat{a}_* changes sign is larger than one. Interestingly, for $\hat{v}_2 \rightarrow 0$ the overlap \hat{a}_* diverges.

2. Mechanical equilibrium

Having determined the chemically stable retrieval states in the limit of sparse target vectors, we now determine their mechanically stable branches. To this aim,

we expand the coefficients c_1 and c_2 that appear in the stability conditions (D14) and (D15) in v_3 , viz.,

$$c_1 = c_1^{(0)} + v_3 c_1^{(1)} + O(v_3^2) \quad (\text{G9})$$

and

$$c_2 = c_2^{(0)} + v_3 c_2^{(1)} + O(v_3^2) \quad (\text{G10})$$

and we determine the above four coefficients from a Taylor expansion in v_3 of the Eqs. (D3) and (D4) in the limit $q \rightarrow 0$.

For the zero-order coefficients, that determine stability at $v_3 = 0$, we get

$$c_1^{(0)} = 1 + e^{-\mu_N} \quad (\text{G11})$$

and

$$c_2^{(0)} = \frac{\hat{a}^{(0)}}{1 + \hat{a}^{(0)}} (1 + e^{-\mu_N}). \quad (\text{G12})$$

Substitution of Eqs. (G11) and (G12) into Eqs. (D14) and (D15), we find that for all values of \hat{v}_2 retrieval states are *not* mechanically stable at $v_3 = 0$. Indeed, for $\hat{v}_2 \leq 1$ it holds that $\hat{a}^{(0)} > 0$, and therefore $c_2^{(0)} > 0$. Consequently, the inequality (D15) determines mechanical stability, which reads here $\hat{a}_*^{(0)} \leq (1 - \hat{v}_2)/\hat{v}_2$, and is not satisfied for $\hat{v}_2 \leq 1$. Analogously, for $\hat{v}_2 \geq 1$ it holds that $\hat{a}^{(0)} < 0$, and therefore $c_2^{(0)} < 0$. Consequently, we require the inequality (D14) that reads $\hat{v}_2 \leq 1$ in the limit $q \rightarrow 0$.

Taken together, retrieval states are not stable for $v_3 = 0$, and we require a nonzero v_3 to stabilise them. The linear-order coefficients in Eqs. (G11) and (G12) read

$$c_1^{(1)} = \frac{2 + 3e^{-\mu_N}}{2(1 + e^{-\mu_N})^2} \quad (\text{G13})$$

and

$$\begin{aligned} c_2^{(1)} &= \frac{e^{-\mu_N}}{2(1 + \hat{a}^{(0)})^2(1 + e^{\mu_N})^2} \\ &\times \left(2\hat{a}^{(1)}(1 + e^{\mu_N})^3 \right. \\ &\left. - \hat{a}^{(0)}(1 + \hat{a}^{(0)})e^{2\mu_N} \left\{ 1 + 2\hat{a}^{(0)} + 2(1 + \hat{a}^{(0)})e^{\mu_N} \right\} \right). \end{aligned} \quad (\text{G14})$$

Substitution of (G11) and (G13) in (D3), and substitution of (G12) and (G14) in (D4), yields expressions for c_1 and c_2 up to linear order in v_3 , which we can substitute in Eqs. (D14) and (D15) to determine the mechanical stability of retrieval states up to linear order in perturbation theory. In Fig. 8, we depict the stable branches of the retrieval state with thick lines, demonstrating that stable retrieval is possible at small values of v_2 when $v_3 > 0$.

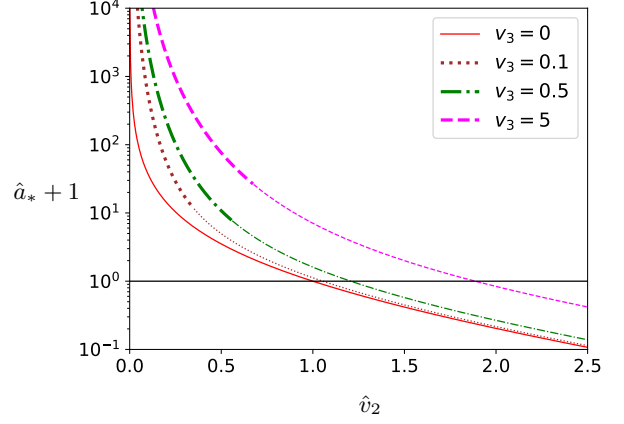


FIG. 8. Plot of the chemically stable value of the overlap $\hat{a}_* = a_*/\sqrt{q}$ of retrieval states at $q = 0$ as a function of $\hat{v}_2 = v_2/(1 + \exp(-\mu_N))$ for small values of v_3 . We used the perturbation theory up to linear order, see (G2), with coefficients determined by the formulae (G7) and (G8). We have set $\mu_N = 1$ and v_3 is given as in the legends. The thick lines and thin lines denote the mechanically stable and unstable branches, respectively. For $v_3 = 0$ the retrieval state is unstable for all values of \hat{v}_2 . The solid horizontal line denotes $\hat{a}_* = 0$ and is a guide to the eye.

In Fig. 9 we plot the lines of marginal stability up to linear order in v_3 . Above these lines, the retrieval state is stable. Importantly, for finite values of v_2 we require a finite v_3 to render retrieval states mechanically stable. Note that according to Fig. 9 stable retrieval states are not possible for large enough values of v_2 , as an infinitely large v_3 is required to stabilise states beyond a finite value of v_2 . However, it should be stressed that this is a perturbative result up to linear orders in v_3 , and we expect this effect to disappear when considering higher orders in perturbation theory.

Appendix H: Numerical methods

We elaborate on the numerical methods used to generate Figures 4 and 5.

The numerical results in these figures are obtained by numerically minimising the extended potential $\omega(\vec{\rho}, \mu^{\text{res}})$ with the truncated Newton method given an initial state $\vec{\rho} = \vec{\rho}^{\text{init}}$. Specifically, the *TNC* algorithm of the *Scipy Optimization library* was used.

The key observable in Fig. 4 is the size of the basin of attraction \mathcal{S} which is a function of the p selected hyper-symmetric target states and a sequence $\vec{\rho}^{\text{init}}(r)$ of initial states, where $r = mN/j$ and $j \in \{1, 2, \dots, m\}$; in the Fig. 4 $m = 50$. The size of the basin of attraction \mathcal{S} is the maximal value of r for which the minimization algorithm converges to the target state (we always consider enough iterations for the minimizer to find a minimum).

We specify how the m initial states $\vec{\rho}^{\text{init}}(r)$ are constructed. The component densities of the initial states

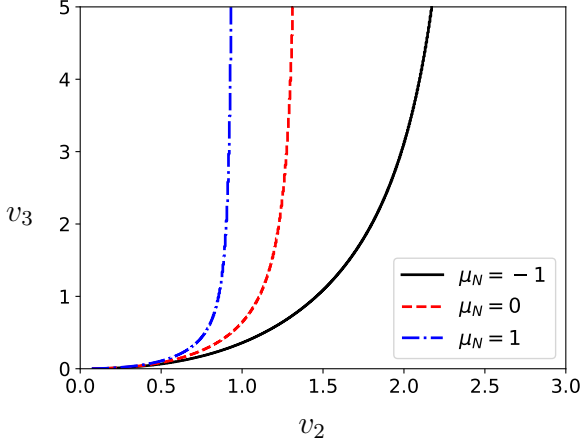


FIG. 9. Lines of marginal stability, separating a stable retrieval state at small values of v_2 from an unstable retrieval state at large values of v_2 , calculated up to linear order in perturbation theory (v_3 being the small parameter) and for $q = 0$. Lines are obtained by using the linear expressions (G9) and (G10) for c_1 and c_2 in the equality of Eq. (D14) [we only find stability in the region with $c_2 > 0$, and thus (D15) is not relevant] evaluated at $q = 0$.

are set to either of three values: a chosen number r of the densities is set to the value ρ_* in the homogeneous state given by Eq. (9); the remaining $N - r$ densities are set to the pair of values given by the target state $\vec{\rho}_*^\alpha$ with component densities ρ_i^α as defined in Eq. (11), and where $a = a_*$ and $\rho = \rho_*$ from Eqs. (12) and (13). The r components with densities ρ_* are selected uniformly at random amongst the N possible component. Moreover, these components are selected independently for different

values of r .

Next, we specify how \mathcal{S} is determined from a given sequence of initial states $\vec{\rho}^{\text{init}}(r)$. For this, we determine the maximal value of r for which the overlap

$$a(\vec{\rho}_*^\alpha, \vec{\rho}^{\text{final}}) = \frac{\sum_{i=1}^N \rho_{*,i}^\alpha \rho_i^{\text{final}}}{\sum_{i=1}^N \rho_i^{\text{final}}} \quad (\text{H1})$$

between the target state $\vec{\rho}_*^\alpha$ and the final converged result $\vec{\rho}^{\text{final}}(r)$ of the minimising algorithm is larger or equal than 0.99, i.e.,

$$\mathcal{S}(\vec{\gamma}^\alpha, \{\vec{\gamma}^\beta\}_{\beta=1,2,\dots,p}; \{\vec{\rho}^{\text{init}}(r)\}_{r=1,2,\dots,m}) = \frac{\max\{r \in \{1, \dots, m\} : a(\vec{\rho}_*^\alpha, \vec{\rho}^{\text{final}}(r)) \geq 0.99\}}{m}.$$

Lastly we specify the meaning of the average value $\langle \mathcal{S} \rangle$. The average is taken over both the random choice of the p hypersymmetric targets, as described in Appendix A, the random choice of the selected target state $\vec{\gamma}^\alpha$, and the random choice of the components of the sequence $\vec{\rho}^{\text{init}}(r)$ that are set equal to ρ_* . In Fig. 4 the average $\langle \mathcal{S} \rangle$ is estimated as an empirical mean over 20 realisations of both the targets and the choice of components that are set equal to ρ_* . Error bars denote the standard deviation on the empirical mean.

For Fig.5, the initial states $\vec{\rho}^{\text{init}}$ for the truncated Newton method applied to ω are generated from the, so-called, flat Dirichlet distribution, which corresponds with a uniform sampling over the the standard simplex. Figure 5A is constructed from 10^6 initial configurations, and each point of Fig.5B is an empirical mean over 10^5 initial configuration points were generated.

-
- [1] R. P. Sear and J. A. Cuesta, Instabilities in complex mixtures with a large number of components, *Physical review letters* **91**, 245701 (2003).
 - [2] A.-C. Gavin, M. Bösche, R. Krause, P. Grandi, M. Marzioch, A. Bauer, J. Schultz, J. M. Rick, A.-M. Michon, C.-M. Cruciat, *et al.*, Functional organization of the yeast proteome by systematic analysis of protein complexes, *Nature* **415**, 141 (2002).
 - [3] P. Sartori and S. Leibler, Lessons from equilibrium statistical physics regarding the assembly of protein complexes, *Proceedings of the National Academy of Sciences* **117**, 114 (2020).
 - [4] C. P. Brangwynne, C. R. Eckmann, D. S. Courson, A. Rybarska, C. Hoeg, J. Gharakhani, F. Jülicher, and A. A. Hyman, Germline p granules are liquid droplets that localize by controlled dissolution/condensation, *Science* **324**, 1729 (2009).
 - [5] A. A. Hyman, C. A. Weber, and F. Jülicher, Liquid-liquid phase separation in biology, *Annu. Rev. Cell Dev. Biol* **30**, 39 (2014).
 - [6] J.-M. Choi, A. S. Holehouse, and R. V. Pappu, Physical principles underlying the complex biology of intracellular phase transitions, *Annual review of biophysics* **49**, 107 (2020).
 - [7] J. Berry, C. P. Brangwynne, and M. Haataja, Physical principles of intracellular organization via active and passive phase transitions, *Reports on Progress in Physics* **81**, 046601 (2018).
 - [8] D. Lingwood and K. Simons, Lipid rafts as a membrane-organizing principle, *science* **327**, 46 (2010).
 - [9] F. A. Heberle and G. W. Feigenson, Phase separation in lipid membranes, *Cold Spring Harbor perspectives in biology* **3**, a004630 (2011).
 - [10] A. Murugan, Z. Zeravcic, M. P. Brenner, and S. Leibler, Multifarious assembly mixtures: Systems allowing retrieval of diverse stored structures, *Proceedings of the National Academy of Sciences* **112**, 54 (2015).
 - [11] W. M. Jacobs and D. Frenkel, Predicting phase behavior in multicomponent mixtures, *The Journal of chemical physics* **139**, 024108 (2013).
 - [12] W. M. Jacobs and D. Frenkel, Phase transitions in biological systems with many components, *Biophysical journal* **112**, 683 (2017).
 - [13] G. Carugno, I. Neri, and P. Vivo, Instabilities of complex fluids with partially structured and partially random interactions, *Physical Biology* **19**, 056001 (2022).

- [14] M. Girard, On kinetics and extreme values in systems with random interactions, *Physical Biology* **20**, 016006 (2022).
- [15] F. C. Thewes, M. Krüger, and P. Sollich, Composition dependent instabilities in mixtures with many components, *Phys. Rev. Lett.* **131**, 058401 (2023).
- [16] D. Zwicker and L. Laan, Evolved interactions stabilize many coexisting phases in multicomponent liquids, *Proceedings of the National Academy of Sciences* **119**, e2201250119 (2022).
- [17] W. M. Jacobs, Self-assembly of biomolecular condensates with shared components, *Physical review letters* **126**, 258101 (2021).
- [18] J. J. Hopfield, Neural networks and physical systems with emergent collective computational abilities., *Proceedings of the national academy of sciences* **79**, 2554 (1982).
- [19] H. B. Callen, *Thermodynamics and an introduction to thermostatistics* (1998).
- [20] S. Safran, *Statistical Thermodynamics Of Surfaces, Interfaces, And Membranes* (CRC Press., 2003).
- [21] M. Doi, *Soft matter physics* (Oxford University Press, 2013).
- [22] S. Mao, D. Kuldinow, M. P. Haataja, and A. Košmrlj, Phase behavior and morphology of multicomponent liquid mixtures, *Soft Matter* **15**, 1297 (2019).
- [23] J. Hertz, A. Krogh, and R. G. Palmer, *Introduction to the theory of neural computation* (CRC Press, 2018).
- [24] K. Shrinivas and M. P. Brenner, Phase separation in fluids with many interacting components, *Proceedings of the National Academy of Sciences* **118**, e2108551118 (2021).
- [25] I. R. Graf and B. B. Machta, Thermodynamic stability and critical points in multicomponent mixtures with structured interactions, *Phys. Rev. Res.* **4**, 033144 (2022).
- [26] B. Kramer and A. MacKinnon, Localization: theory and experiment, *Reports on Progress in Physics* **56**, 1469 (1993).
- [27] K. Efetov, *Supersymmetry in disorder and chaos* (Cambridge university press, 1999).
- [28] M. V. Tsodyks and M. V. Feigel'man, The enhanced storage capacity in neural networks with low activity level, *Europhysics Letters* **6**, 101 (1988).
- [29] K. Simons and D. Toomre, Lipid rafts and signal transduction, *Nature reviews Molecular cell biology* **1**, 31 (2000).
- [30] P. A. Chong and J. D. Forman-Kay, Liquid-liquid phase separation in cellular signaling systems, *Current opinion in structural biology* **41**, 180 (2016).
- [31] Y. Shin and C. P. Brangwynne, Liquid phase condensation in cell physiology and disease, *Science* **357**, eaaf4382 (2017).
- [32] S. F. Banani, H. O. Lee, A. A. Hyman, and M. K. Rosen, Biomolecular condensates: organizers of cellular biochemistry, *Nature reviews Molecular cell biology* **18**, 285 (2017).
- [33] K. G. Murty and S. N. Kabadi, *Some NP-complete problems in quadratic and nonlinear programming*, Tech. Rep. (1985).
- [34] P. M. Pardalos and G. Schnitger, Checking local optimality in constrained quadratic programming is np-hard, *Operations Research Letters* **7**, 33 (1988).
- [35] P. M. Pardalos and S. A. Vavasis, Quadratic programming with one negative eigenvalue is np-hard, *Journal of Global optimization* **1**, 15 (1991).
- [36] M. Mézard, G. Parisi, and M. A. Virasoro, *Spin glass theory and beyond: An Introduction to the Replica Method and Its Applications*, Vol. 9 (World Scientific Publishing Company, 1987).
- [37] P. Charbonneau, E. Marinari, G. Parisi, F. Ricci-Tersenghi, G. Sicuro, F. Zamponi, and M. Mezard, *Spin Glass Theory and Far Beyond: Replica Symmetry Breaking after 40 Years* (World Scientific, 2023).
- [38] J. J. Hopfield, Neurons with graded response have collective computational properties like those of two-state neurons., *Proceedings of the national academy of sciences* **81**, 3088 (1984).
- [39] D. Bollé, T. M. Nieuwenhuizen, I. P. Castillo, and T. Verbeiren, A spherical hopfield model, *Journal of Physics A: Mathematical and General* **36**, 10269 (2003).
- [40] P. N. McGraw and M. Menzinger, Bistable gradient networks. i. attractors and pattern retrieval at low loading in the thermodynamic limit, *Phys. Rev. E* **67**, 016118 (2003).
- [41] P. N. McGraw and M. Menzinger, Bistable gradient networks. ii. storage capacity and behavior near saturation, *Phys. Rev. E* **67**, 016119 (2003).
- [42] C. G. Evans, J. O'Brien, E. Winfree, and A. Murugan, Pattern recognition in the nucleation kinetics of non-equilibrium self-assembly, *arXiv preprint arXiv:2207.06399* (2022).
- [43] A. Hedayat and W. D. Wallis, Hadamard matrices and their applications, *The Annals of Statistics* , 1184 (1978).